Scientific Drilling
Open Access

Scientific drilling of sediments at Darwin Crater, Tasmania

Agathe Lisé-Pronovost[1,2]**, Michael-Shawn Fletcher**[3]**, Tom Mallett**[2]**, Michela Mariani**[3,4]**, Richard Lewis**[5]**,
Patricia S. Gadd**[6]**, Andy I. R. Herries**[2]**, Maarten Blaauw**[7]**, Hendrik Heijnis**[6]**, Dominic A. Hodgson**[8,9]**, and
Joel B. Pedro**[10]

[1]School of Earth Sciences, University of Melbourne, Melbourne, Australia
[2]The Australian Archaeomagnetism Laboratory, Department of
Archaeology and History, La Trobe University, Melbourne Campus,
Bundoora, 3086, VIC, Australia
[3]School of Geography, University of Melbourne, Melbourne, Australia
[4]School of Geography, University of Nottingham, Nottingham, UK
[5]School of Earth and Environmental Sciences, University of Adelaide, Adelaide, SA, Australia
[6]Australian Nuclear Science and Technology Organisation, Lucas Heights, NSW, Australia
[7]School of Natural and Built Environment, Queen's University Belfast, Belfast, UK
[8]British Antarctic Survey, Cambridge, CB3 0ET, UK
[9]Department of Geography, University of Durham, Durham DH1 3LE, UK
[10]Antarctic Climate and Ecosystems CRC, University of Tasmania,
Hobart, 7001, TAS, Australia

Correspondence: Agathe Lisé-Pronovost (agathe.lise@unimelb.edu.au)

Abstract. A 70 m long continental sediment record was recovered at Darwin Crater in western Tasmania, Australia. The sediment succession includes a pre-lake silty sand deposit overlain by lacustrine silts that have accumulated in the ∼ 816 ka meteorite impact crater. A total of 160 m of overlapping sediment cores were drilled from three closely spaced holes. Here we report on the drilling operations at Darwin Crater and present the first results from petrophysical whole core logging, lithological core description, and multi-proxy pilot analysis of core end samples. The multi-proxy dataset includes spectrophotometry, grain size, natural gamma rays, paleo- and rock magnetism, loss on ignition, and pollen analyses. The results provide clear signatures of alternating, distinctly different lithologies likely representing glacial and interglacial sediment facies. Initial paleomagnetic analysis indicate normal magnetic polarity in the deepest core at Hole B. If acquired at the time of deposition, this result indicates that the sediment 1 m below commencement of lacustrine deposition post-date the Matuyama–Brunhes geomagnetic reversal ∼ 773 ka.

1 Introduction

Pleistocene glacial and interglacial cycles involved repeated massive reorganisations of the Earth system. Proxies in ocean, ice-core, and continental records capture a range of these changes at global to regional and local scales. Continental records show how terrestrial environments responded to the large-scale shifts between glacial and interglacial states, providing valuable insights into the interactions between the atmosphere, oceans, cryosphere and biosphere, and the long-term context from which to interpret current and future trends. This is particularly important in the mid- to high latitudes of the Southern Hemisphere, where Antarctic climate and circumpolar atmosphere–ocean dynamics exert a dominant influence not only on southern terrestrial climates but also on the global carbon cycle (Saunders et al., 2018; Skinner et al., 2010; Toggweiler, 2009; Toggweiler et al.,

2006). These studies highlight the role of the Southern Hemisphere westerly winds (SWWs) in regulating the Southern Ocean carbon sink and the global carbon cycle. Empirical data from long paleoclimate records are therefore needed to test different theories of how the Earth system operates and if they can be simulated in Earth system models.

Crater lake sediment records often have great scientific value and can provide local to global climate histories (e.g. Wilke et al., 2016). Examples of impact craters with lacustrine sediment records include Bosumtwi in Ghana (6°30′ N; 1 Ma; Scholz et al., 2007), Colônia in Brazil (23°52′ S; 5 Ma; Ledru et al., 2015), El'Gygytgyn in Russia (67°30′ N; 2.8 Ma; Melles et al., 2012), and Pingualuit in Canada (61°16′ N; 1.4 Ma; Guyard et al., 2011). There is, to date, no sediment record from an impact crater in the mid-latitudes of the Southern Hemisphere, however there are volcanic crater sediment records, such as Potrok Aike in south-eastern Patagonia (51°58′ S; 107 m; 51 ka; Zolitschka et al., 2013), Lake Pupuke in New Zealand (37°47′ S; 48 ka; Stephens et al., 2012), and a series of volcanic craters in the Newer Volcanics Province in south-eastern Australia (∼ 38°; Matchan et al., 2017 and references therein). Long Pleistocene lake sediment records are extremely rare in Australia because of the aridity and the general absence of glaciers and recent tectonic activity able to form deep freshwater basins. Many mainland Australian lakes are ephemeral, and very few originate from before the last glacial period (Falster et al., 2018). Exceptions include discontinuous paleo-lakes in mainland Australia, such as Stony Creek basin (37°21′ S; 1.85–1.55 Ma; Sniderman et al., 2007) and mega-lake Bungunnia (∼ 35° S; 2.5–0.8 Ma; McLaren and Wallace, 2010), and glacial lakes extending back to the last glacial in Tasmania (Beck et al., 2017; Colhoun, 2000; Colhoun et al., 1999). Our knowledge of Pleistocene climate in Australia is therefore incomplete.

Here we report on the drilling operations at Darwin Crater, a ∼ 816 ka old meteorite impact crater in western Tasmania, Australia (42°18′ S, 145°39′ E). Drilling at Darwin Crater 40 years ago recovered 60 m of lacustrine sediments overlying 160 m of coarser crater-fill deposits, including polymictic and sandy unconsolidated breccia overlying deformed slates (Howard and Haines, 2007). While low-resolution pollen data were compiled on the upper 20 m of that core, revealing excellent pollen preservation and clear shifts between glacial and interglacial vegetation and climate (Colhoun and van der Geer, 1998), little further analyses were completed or published from this important archive. A note on paleomagnetic polarity of the original core by Barton (1987) in congress proceedings stated that the base of the Darwin lake sediments was of normal polarity, however no paleomagnetic data were published. Here, we present the first results from a new drilling campaign at Darwin Crater in 2018. The aim of this drilling was to recover the lacustrine sediment sequence (the uppermost 60 m of sediments in the crater) to bridge a time gap in the Australian paleoclimate record and provide a long continental record of Pleistocene climate in the mid-latitudes of the Southern Hemisphere. The results include data from non-destructive whole core logging (natural gamma ray, magnetic susceptibility, and resistivity) and multi-proxy pilot analysis of core end samples (spectrophotometry, grain-size, magnetic, loss-on-ignition, and pollen analyses). We interpret this data and outline the ongoing and potential future research directions.

2   Drilling target and geological settings

Darwin Crater is a 1.2 km diameter unconfirmed meteorite impact crater in western Tasmania, Australia (42°18′13″ S, 145°39′36″ E; Fig. 1). Gravity and magnetic surveys and scientific drilling in 1975 and 1983 revealed that the circular depression is filled with 60 m of lake sediments overlying 40 m of mixed muds, sands and rock fragments (unconsolidated breccia) and 120 m of deformed, brecciated, slumped, and fractured slate and quartzite laying over coherent local slate (Richardson, 1984; Howard and Haines, 2007). The stratigraphy is consistent with a small simple impact crater, however it is unconfirmed, because no diagnostic shock indicators have been found (Howard and Haines, 2007). The impactite "Darwin glass" is found within a 400 km^2 strewn field around Darwin Crater, where it most likely originates (Fudali and Ford, 1979; Howard and Haines, 2007; Howard, 2009) and is dated at 816 ± 7 ka by ^{40}Ar/^{39}Ar (Lo et al., 2002). Darwin glass is frequently found in archaeological cave sites in the region because this sharp and resistant material was used as a cutting tool by Aboriginal Tasmanians during the Pleistocene (Allen et al., 2016).

Darwin Crater lies 170 m above sea level, and the lake that formerly occupied the crater drained a small catchment area of 2.2 km^2 (Fig. 1d). The regional geology is dominated by sedimentary rocks and Quaternary deposits in the valley around the crater, volcanic and volcaniclastic rocks to the north-west (e.g. Mount Darwin, Mount Sorell), and quartzite to the east (e.g. Frenchman's Cap in the Engineer Range). The modern climate is cool temperate, with mean annual temperatures at nearby Queenstown (20 km distant) ranging from 5.6–16.4 °C and with 2405 mm rain per year (Australian Bureau of Meteorology). The climate is dominated by the SWWs which, together with orography, control precipitation in Tasmania and throughout the mid- to high latitudes of the Southern Hemisphere (Fig. 1b) (Garreaud, 2007). The crater is vegetated with shrubs, sedges, and grasses (including *Melaleuca squamea*, *Leptospermum* spp., *Monotoca glauca*, *Gymnoschoenus sphaerocephalus*, and *Restio australis*) occupying the basin floor, whilst the surrounding slopes are occupied by a cool temperate rainforest assemblage including *Lagarostrobos franklinii*, *Nothofagus cunninghamii*, and *Phyllocladus aspleniifolius*.
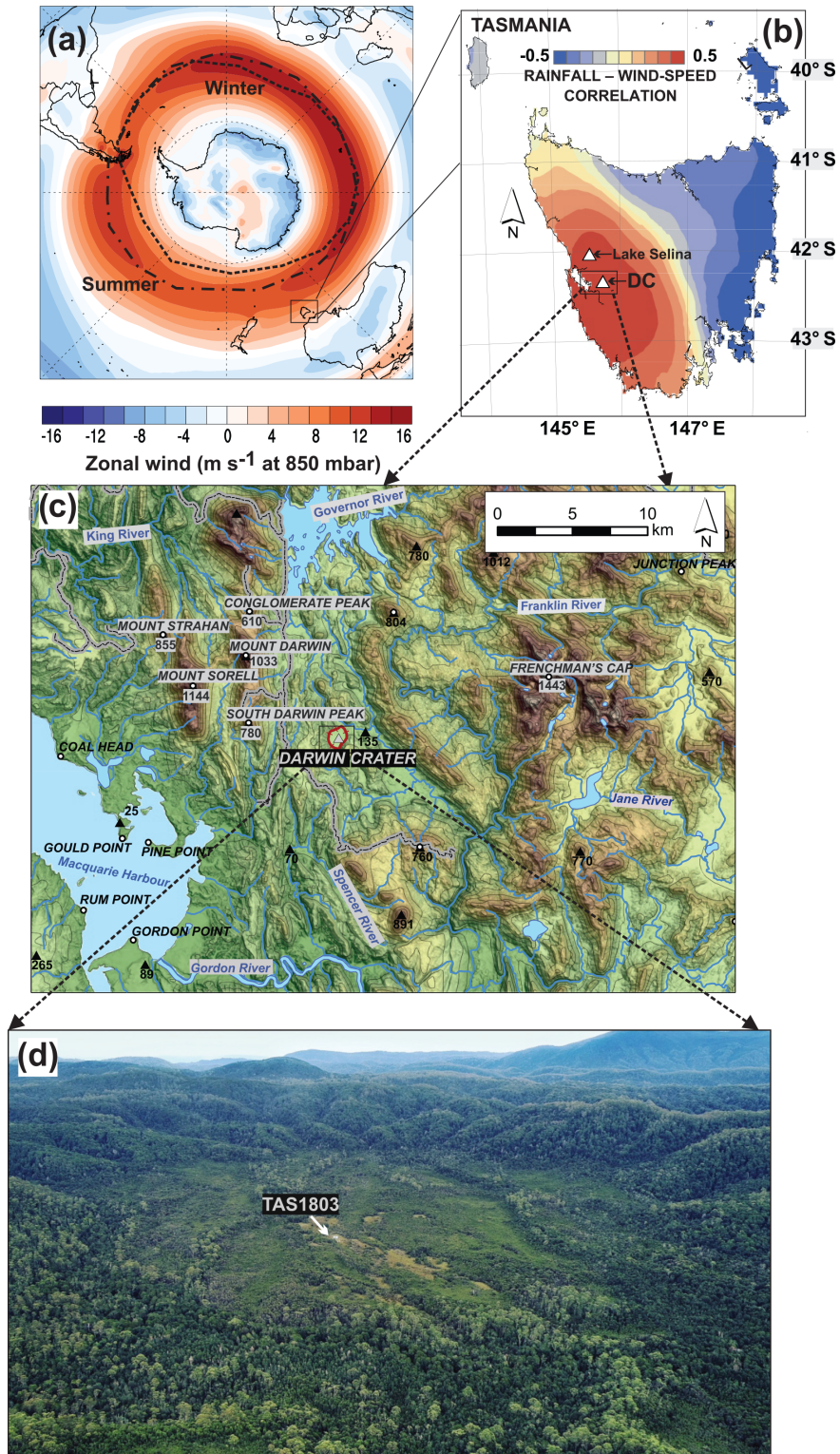
Figure 1. (a) Zonal wind speed at 850 mbar in the mid-latitude of the Southern Hemisphere, and average winter and summer core position of the Southern Hemisphere westerly winds (SWWs). **(b)** The SWWs are a dominant climate control in western Tasmania, where rainfall is strongly correlated to wind intensity and orography. **(c)** Regional topographic map showing the location of Darwin Crater, and **(d)** aerial oblique drone image of Darwin Crater during the scientific drilling operations in April 2018. The drill and camp site are visible in white. Wind data from the NCEP and NCAR Reanalysis V1 (Kalnay et al., 1996).

3   Drilling operations

The scientific drilling operations at Darwin Crater took place on 18–25 April 2018. The drill team was composed of six people, including two drillers, two students, and two researchers. Darwin Crater is in the remote Tasmanian Wilderness World Heritage Area. While a road was bulldozed to access the crater for drilling in the 1970s, today the crater is inaccessible by road. Therefore, the team, drill rig, camp, and equipment were transported to the site by helicopter (Fig. 2a–b).

The drill site TAS1803 (Fig. 1d; $42°18'16.46''$ S, $145°39'33.09''$ E) was selected in the approximate centre of the paleolake and in open sedgeland vegetation to facilitate camp set-up. Three parallel holes were drilled using a Boart Longyear 47 drill rig and HQ pipes (96 mm outside and 63.5 mm inside diameter) with a diamond drill bit (Fig. 3d). The same tools were used for all cores drilled. Core catchers were only required in the first few runs of Hole A because sediment lower down the sequence were sufficiently cohesive to be retained in the tube without loss. The drill rig was pushed 1.1 m eastward from Hole A to Hole B and 1.3 m eastward from Hole B to Hole C. The sediment recovery was initially low in the upper half of Hole A as we worked on establishing the best method for sediment retention. The optimal method proved to involve minimal flushing with water and rotation of the core barrel to allow efficient recovery of the poorly consolidated lake sediments. Once the optimal method was identified, operations went smoothly, and Hole B was successfully drilled the next day with 95.6 % recovery (Table 1). Holes A and B were abandoned when the top of the pre-lake crater infill described by Howard and Haines (2007) was reached, which indicated that the full lake sediment sequence had been successfully recovered. Hole C was drilled to ca. 44 m to obtain full overlap of the uppermost part of the record, which had lower recovery than the lower part of the record (Table 1).

Cores were retrieved in standard 10 ft long (3.048 m) transparent PVC HQ wire-line core liners. Each core was immediately wrapped in black plastic foil to protect from sunlight and allow for future optically stimulated luminescence (OSL) dating analyses (Fig. 2c). The core end sediments that protruded from the core liners or those retained in the core catchers (up to 6.5 cm) were collected in labelled bags (Fig. 2e–g) for preliminary analyses. Each 3 m core was cut into ca. 150 cm sections to facilitate transport and storage (total 93 core sections). We use the nomenclature "-TM" for the top to middle and "-MB" for the middle to base sections (e.g. core TAS1803-B10 is cut into TAS1803-B10-TM and TAS1803-B10-MB). Cores are stored in cold rooms and curated at the University of Melbourne within the School of Geography. All data will be deposited upon publication in the National Oceanic and Atmospheric Association (NOAA), NEOTOMA (https://www.neotomadb.org/, last ac-

Table 1. Summary of holes drilled and core recovery at Darwin Crater site TAS1803.

Hole	Start (m)	End (m)	Drilled (m)	Recovered (m)	Recovery (%)
A	1.66	70.76	69.10	55.39	80.2
B	0.56	69.26	68.70	65.66	95.6
C	0	43.66	43.66	39.58	90.7
Total			181.5	160.6	

cess: 11 January 2019), and PANGAEA (https://pangaea.de/, last access: 11 January 2019) public data repositories.

4   Core scanning and multi-proxy analyses of core end samples

Whole core scanning of non-destructive petrophysical properties was performed using a Geotek Multi-Sensor Core Logger (MSCL) for all cores from Holes A, B, and C, in the Petrophysics Laboratory at the University of Melbourne. Volumetric magnetic susceptibility in low field (k_{LF}; 0.565 kHz) was measured using a Bartington MS2C loop sensor with a diameter of 8 cm, and the non-contact resistivity was measured using a Geotek sensor at 1 cm intervals. Natural gamma ray (NGR) emission integrated over 20 cm of core was counted for 1 min using Geotek NaI(Tl) at 40 cm intervals on the cores from Hole A.

The cores from Hole B were split lengthwise using a Geotek core splitter. Core splitting was conducted under red light, and one core half was wrapped in black plastic foil and stored at 4 °C for OSL and paleomagnetic sampling. The other half was used for visual lithological core descriptions and sent to Australia's Nuclear Science and Technology Organisation (ANSTO) for micro-XRF (Itrax) core scanning and core photography. The scanned half will be subsampled for multi-proxy analysis (including pollen, charcoal, grain size, magnetic properties, and aDNA). These procedures are repeated for the cores from each hole.

The core end samples from Holes A, B, and C (total 57 samples) were analysed for their magnetic properties, spectrophotometry, grain size, and loss on ignition, while only select core end samples were analysed for pollen.

Room-temperature magnetic measurements were performed at The Australian Archaeomagnetism Laboratory at La Trobe University to characterise the magnetic mineral assemblage and evaluate the potential for changes in the paleomagnetic field to provide a geochronological tool. Standard 8 cm^3 paleomagnetic boxes (unoriented) were used for all the core end samples from Holes A, B, and C. In addition, four box samples (A20, A21, B9, and B10) were taken partially oriented from well-preserved cylinder-shaped core ends (known vertical z axis), and four contiguous cubes were taken oriented (1, 2, 3, and 4) in the deepest core of
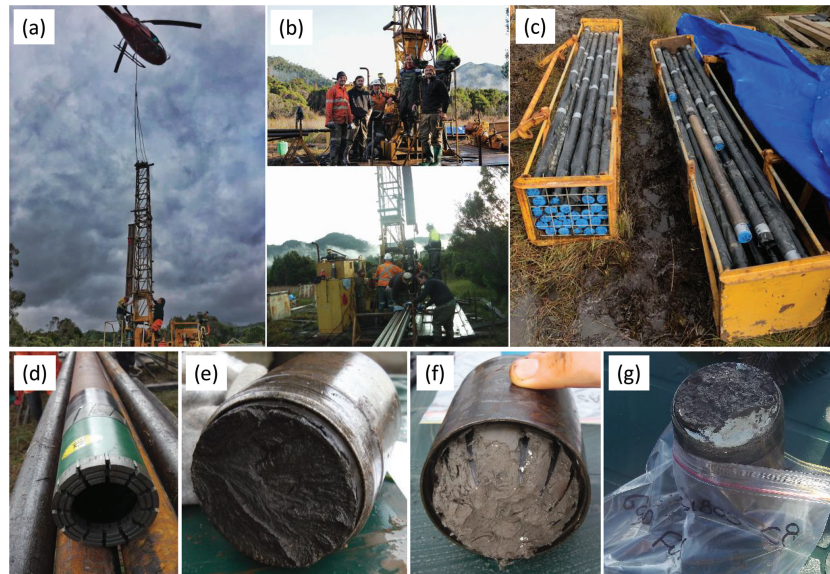
Figure 2. Photos of TAS1803 scientific drilling at Darwin Crater. **(a)** Helicopter-assisted drill rig assembly. **(b)** The drill team and view of the drilling and core handling set-up. **(c)** After recovery, the cores were immediately wrapped in black plastic to protect from light to allow for OSL dating. **(d)** The drill bit, **(e)** core end view from the top, **(f)** core end view from the base, together with the core catcher, and **(g)** core end sample C8 includes a white mineral tentatively identified as vivianite.
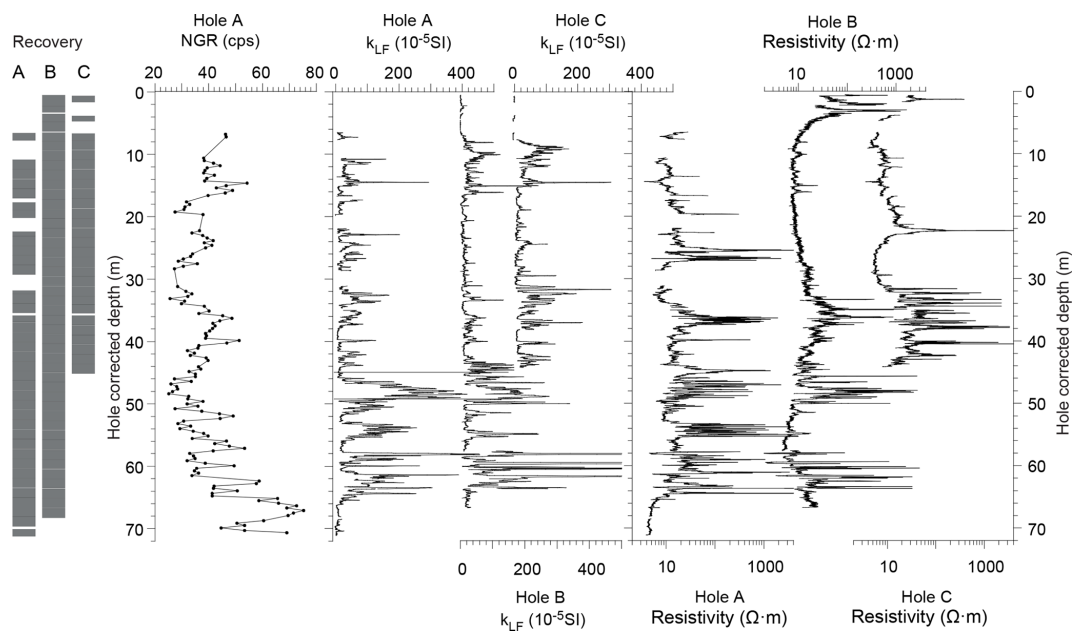
Figure 3. Core recovery log for each core hole and whole core MSCL-scanning data. Grey indicates full recovery, and white indicates no recovery. Natural gamma ray (NGR) was measured at 40 cm intervals, and volumetric magnetic susceptibility (k_{LF}) and resistivity were measured at 1 m intervals.

Hole B (section TAS1803-B-23MB). Magnetic susceptibility was measured using a Bartington MS2B sensor, and the natural and laboratory-induced (anhysteretic in peak alternating field (AF) 0.1 T with 0.05 mT DC biasing field and isothermal in 0.3 T and 2 T DC field) remanent magnetisations (NRM, ARM, and IRM) were acquired using an AGICO

AF Demagnetizer LDA5, an AGICO Magnetizer PAM1, a Magnetic Measurements Pulse Magnetizer MMPM10, and an AGICO JR-6 Spinner Magnetometer. Demagnetisation data were analysed using the Demagnetization Analysis in Excel (DAIE) workbook (Sagnotti, 2013). Finally, first-order reversal curves (FORC) were acquired for three samples us-

ing a LakeShore VSM8600 Vibrating Sample Magnetometer to investigate the magnetic domain state. The FORCs were processed in Forcinel 3.0 (Harrisson and Feinberg, 2008) using VARIFORC smoothing (Egli, 2013).

Quantitative sediment colour (L^*, a^*, and b^*) was acquired using a handheld Konica Minolta CM-700d Spectrophotometer applied directly on the sediments of the paleomagnetic box samples.

Grain-size analysis was carried out on all the core end samples from Holes A, B, and C using a Beckman Coulter LP13320 particle sizer at the School of Geography at the University of Melbourne. Samples were pre-treated with hydrogen peroxide (10 %–30 %) for at least 4 weeks until organic-matter digestion was complete. Sediments were then treated with a dispersing agent, sodium pyrophosphate, and sonicated for at least 5 min prior to analysis. The statistical grain-size parameters were calculated with the GRADISTAT software (Blott and Pye, 2001).

Loss-on-ignition (LOI) analysis was performed on all core end samples using standard techniques, which involved sequential temperature treatments of 1 cc sediment to ascertain water content (60 °C overnight), carbonate content (950 °C for 2 h), and organic content in two parts (360 °C for 24 h for labile carbon; 550 °C for 4 h for black carbon; Heiri et al., 2001). The residual sediment after temperature treatments is an inorganic fraction that may include siliciclastic material, diatoms, oxides and sulfides, and it is herein after referred to as the siliciclastic fraction.

Pollen analysis was performed on the 20 core end samples of Hole B following standard techniques (Faegri and Iversen, 1989), with a set volume (0.5 cc) of sediment sieved with a 100 µm sieve, followed by sequential acid and alkali treatments (KOH, HCl, HF, and acetolysis) to isolate the pollen, spores, and other palynomorphs from the sediment matrix. Pollen and spore counts were then tallied to a minimum count of 300 pollen grains of terrestrial origin under 400X and 630X magnification. An exotic marker was added to each sample to allow calculation of pollen, spore, and other palynomorph (e.g. *Botryococcus*, microscopic charcoal, and pyrite spherules) concentrations.

Principal component analysis (PCA) of selected core end data (pollen, LOI, grain size) was performed to identify relationships between these variables. The data were first normalised to the standard deviation to meet the requirements of data normality required by PCA.

5   Initial results

5.1   Core scanning

The drilled depths and recovery information (Table 1) were combined with the MSCL data to derive a common depth scale ("hole corrected depth" used in Figs. 3, 4, and 8). Recovery gaps were generally assumed to occur at the base of core drives, except for the compaction of peat which resulted

in sediment gaps at the hole top (Hole A – unknown; Hole B – 56 cm; Hole C – 70 cm). In most cases, the top depth of the MSCL data from each core section sequentially follows the base depth of the previous core section. If the previous core section had sediment gap, the top depth of MSCL core data was set at the measured drilling depth. The Hole corrected depth did not include the core end thickness (sediment in the core end), which ranged from 0 to 6.5 cm per drilled core (3 m). The difference between the drilled depth and the hole-corrected depth and core end thickness can be attributed to sediment expansion. Hole B depth was further corrected to account for sediment gaps seen in core sections during splitting (nine sections had gaps ranging from 2–8 cm) and thus constitutes the most representative depth with respect to the sediments accumulated in the crater.

The whole core MSCL-scanning results are presented in Fig. 3. The NGR displays small amplitude variations, with higher values of naturally occurring gamma radiation reflecting a higher content of mineral phases rich in potassium (K), uranium (U), and thorium (Th), such as clay minerals and K feldspar. The magnetic susceptibility (k_{LF}) values display a series of sharp and large amplitude changes and good reproducibility of depth between smoothed records from the three holes (Fig. 4). k_{LF} varies by more than 2 orders of magnitude, which indicates large changes in the concentrations of ferrimagnetic minerals. Intervals with high k_{LF} values generally correspond to low NGR values, especially in the lower section of the core (ca. 65–45 m). A series of peaks in k_{LF} of up to ca. 1000×10^{-5} SI were measured in the lowermost portion of the core from Hole B (Fig. 3). Such high values are not observed in the parallel core from Hole A and hint at possible differential post-depositional diagenesis, chemical precipitation or differential preservation of iron oxides in the different cores. The resistivity values vary mostly between 5–500 Ωm, which is a small range relative to the full range of variability found in geological samples (0.01–10 000 Ωm; Gueguen and Palciauskas, 1994). The resistivity over that range of values has two main controls: the porosity of the material (clays having lower values than sands), and the water content (Gueguen and Palciauskas, 1994). The intervals with consistent inter-hole resistivity primarily reflect the sediment porosity. The intervals with different resistivity behaviours (Fig. 4) reflect variable water content of the sediment and are useful for identifying potential minor disturbances in individual core sections from drilling operations, transport and handling of the cores.

5.2   Core description

The simplified lithology for Hole B (Fig. 4a) is based on visual observations of split core surfaces. The transition from the pre-lake sediment (unconsolidated sand-dominant breccia) to lake sediment is at ∼ 65 m and is marked by a shift to higher magnetic susceptibility and lower NGR values (Fig. 3). The lake sediment unit is 61 m thick and is capped
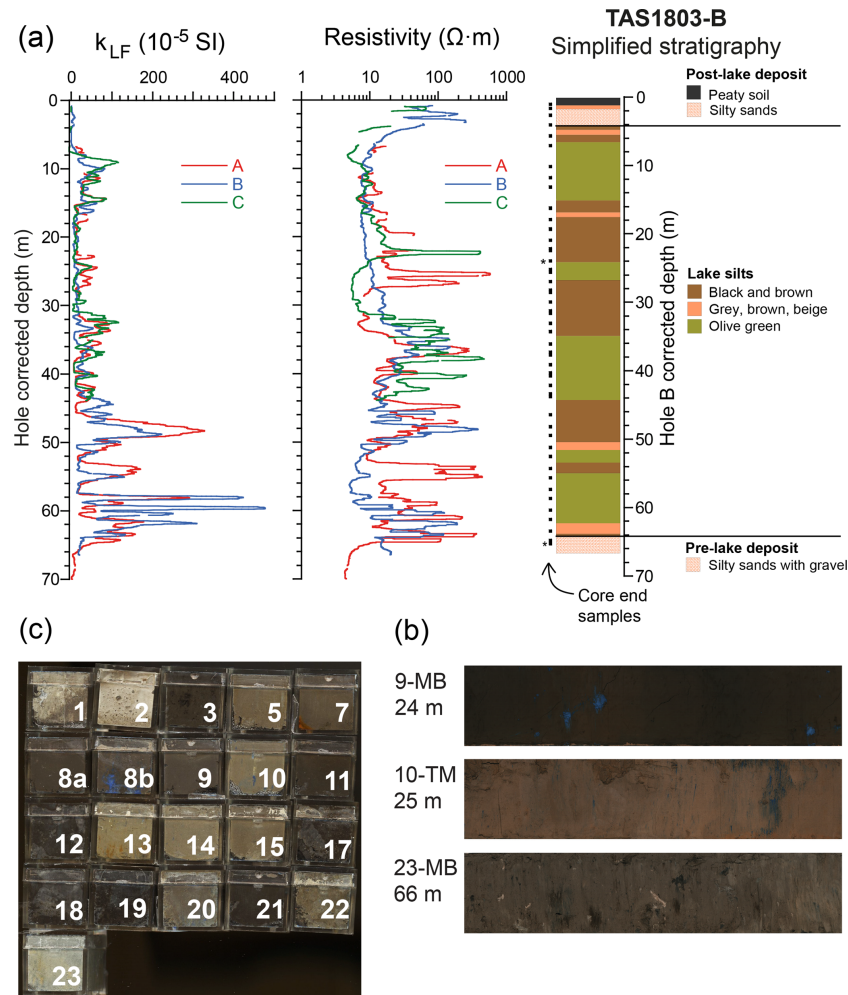
Figure 4. (a) Superimposed plots of volumetric magnetic susceptibility (k_{LF}) and resistivity data from Holes A, B, and C (smoothed over 50 data points), and simplified stratigraphy of site TAS1803 Hole B, which was split in half lengthwise, visually described, and photographed. The position of the core end samples and the paleomagnetic samples in Fig. 6 are indicated with square and asterisk (*), respectively. **(b)** Core end cube samples from Hole B, and **(c)** representative lithologies for black-brown silt (section 9-MB), olive-green silt (section 10-TM) and pre-lake deposits (section 23-MB). The blue mineral visible in sections 9-MB and 10-TM, and cubes 8b and 10 is tentatively identified as vivianite.

by a ∼ 3 m thick coarse-grained clastic layer followed by a ∼ 1 m thick peaty soil layer. The lake sediment is primarily composed of alternating black-brown and olive-green muds with gradual colour transitions. There are occasional sharp contacts between these lithologies and grey muds, mottled muds, and sandy layers. The sediment displays occasional vertical structures interpreted as drilling disturbances or deformation from pressure release between sediment layers of different densities.

Deposits of a white mineral, ranging from very small "specks" to structures > 3 cm in size (Figs. 2g and 4b–c), occur throughout the cores, in both black-brown and olive-green lake sediment units. These minerals were observed changing colour from white to blue upon contact with air (oxidation) and to bright yellow upon contact with a solution of ammonium molybdate and nitric acid. This indicates that it is a phosphate mineral that we tentatively identify as authigenic vivianite, which can form in organic and iron-rich lake sediments under reducing conditions (Rothe et al., 2016). Vivianite constitutes a promising target for uranium series dating (Goetz and Hillaire-Marcel, 1992; Nuttin et al., 2013).

5.3 Core end sample analyses

5.3.1 Physical properties (spectrophotometry and grain size)

The lake sediment deposit has distinctively finer grain sizes (48 samples; fine to coarse silts with mean size of 20 μm) than the pre-lake deposit (three samples; silty sands and sandy silts with mean size of 102 μm) and the post-lake de-
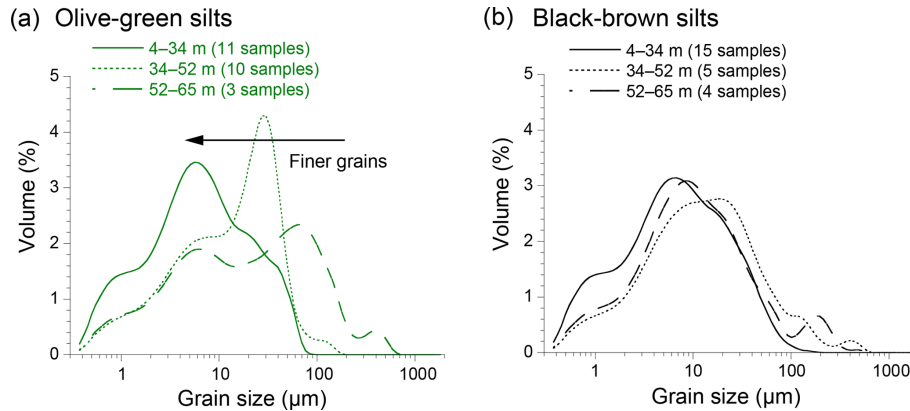
Figure 5. Mean grain-size distribution for the two main types of lake sediments at Darwin Crater. **(a)** Olive-green silts and **(b)** black-brown silts. Shifts to finer grain sizes in olive silts at 52 and 34 m define three depth intervals.

posit (three samples; silty sands and sandy silts with mean size of 167 µm) and has higher L^* values (darker colour). Within the lake sediment unit, L^* (black to white) and b^* (blue to yellow) have distinct values for the two principal lithotypes, with relatively lower L^* and b^* values in the black-brown silts and higher L^* and b^* values in the olive-green silts (Fig. 8d–e). The lake sediment succession above 34 m is more fine grained (fine silts with mean size of 12 µm; 26 samples) than the lowermost part (coarse silts with mean size of 28 µm; 22 samples). Figure 5 illustrates that this shift to finer grains is attributable to the olive-green silts. The mean grain-size distribution of olive-green silts in the uppermost part of the lacustrine sediment succession (4–34 m; solid line in Fig. 5a) is comparable to that of the black-brown silts (Fig. 5b); however, distinctively coarser grain sizes are present in the olive-green silts of the lowermost part (34–65 m; dashed lines in Fig. 5a).

5.3.2 Pollen

A total of 114 different pollen, spore, and palynomorphs were identified in the core end samples from drill Hole B. Overall, the pollen spectra are characterised by either (1) a high proportion of cold climate indicators (Poaceae, Asteraceae, and alpine taxa), including *Tubuliforidites pleistocenicus*, which is now palynologically extinct, and an Asteraceae pollen grain known only from glacial stage pollen flora in south-eastern Australia (Macphail et al., 1993) or (2) a high proportion of warm climate indicators (rainforest plants such as *Lagarostrobos franklinii*, *Nothofagus cunninghamii*, and *Phyllocladus aspleniifolius*; Fletcher and Thomas, 2007). While the coarse resolution of the pollen data currently precludes alignment of the record with glacial-to-interglacial climate shifts, observed variability in pollen abundance clearly reflect shifts between cooler and warmer periods.

5.3.3 Loss on ignition

LOI results reveal high detrital siliciclastic contents in the TAS1803 sediment succession, with values ranging from 38 % to 97 % and an average value of 80 %. The total organic carbon content varies between 1 % and 61 %. Carbonate content is consistently < 4 % for all core end samples.

5.3.4 Magnetic properties

The room-temperature magnetic properties indicate complex magnetic mineral assemblages. The concentration-dependant parameters display large amplitude changes (k_{LF}, χ, NRM, ARM, IRM), with low χ values characteristic of greigite, pyrrhotite, goethite, and hematite as well as high values indicative of magnetite, titanomagnetite, and maghemite (Peters and Dekkers, 2003). The magnetic assemblage is dominated by low-coercivity minerals, as indicated by mostly saturated samples in 0.3 T field (average $IRM_{0.3\,T}$ / $IRM_{2\,T}$ value of 0.96). The magnetic grain-size indicators (SIRM / k_{LF}, kARM / k_{LF}, and ARM / IRM) display different behaviours at times that indicate non-uniform down-core magnetic mineralogy. Stepwise alternating field (AF) demagnetisation of the lake sediment samples (cubes B9t, B10t, A20t, A21t, B23-MB-1, and B23-MB-4; at 2444, 2743, 5896, 6201, 6523, and 6531 cm hole-corrected depth) reveal a stable and well-defined component of NRM (Fig. 6) and the presence of high coercivity minerals (10 %–40 % of NRM remaining after AF 60 mT) and greigite (gyroremanent magnetisation; Fig. 6a; Roberts et al., 2011).

5.3.5 Principal component analysis

The first two PCA axes accounted for 55 % of the variance within the pollen, LOI, and grain-size data. PCA axis 1 (37 % explained variance) separates samples with high siliciclastic content, coarser grain size, and cold climate pollen taxa from samples with high organic content, finer grain size,
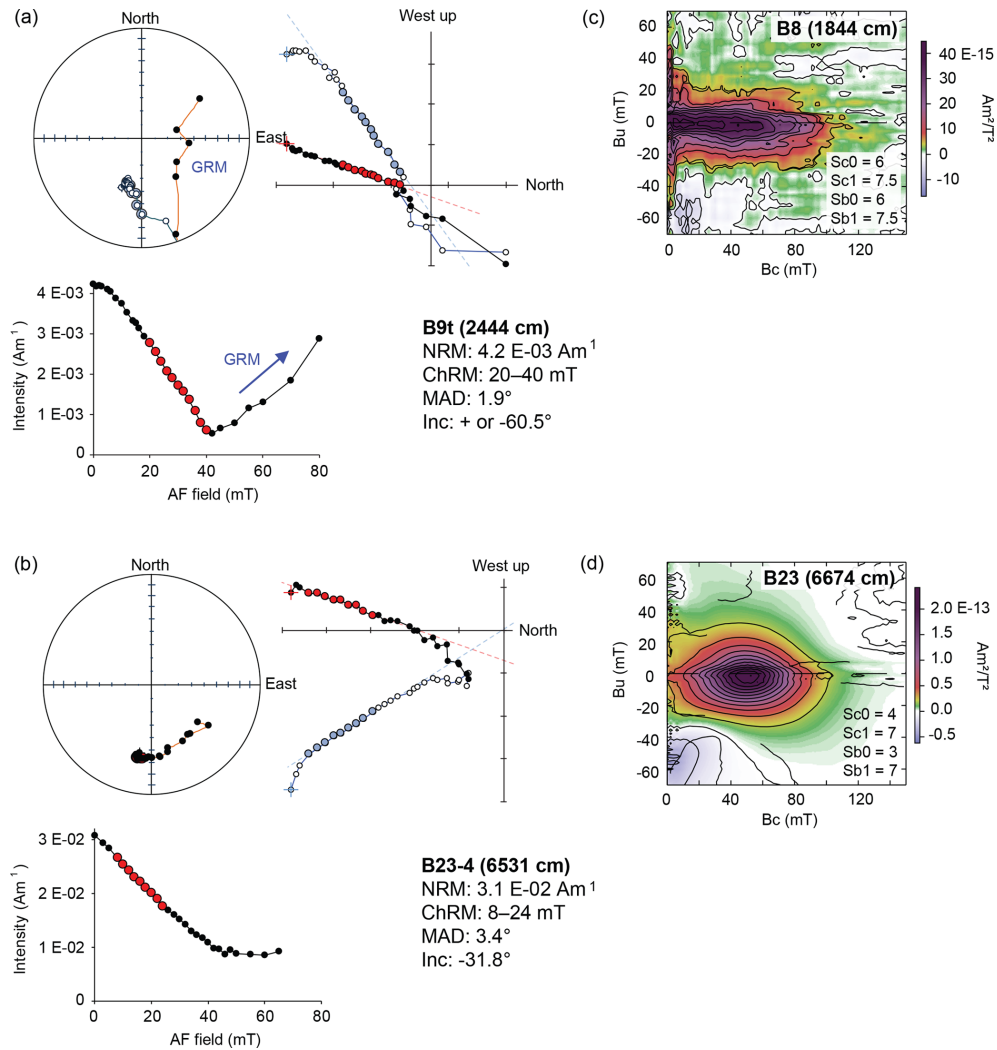
Figure 6. Selected paleo- and rock-magnetic results. Orthogonal projections and alternating field demagnetisation plot for **(a)** lake sediment sample B9t, and **(b)** oriented pre-lake sediment sample B23-4 displaying normal polarity. The down-core position of the samples are indicated by an asterisk in Fig. 5. The acquisition of gyroremanence (GRM) in AF >40 mT is typical of greigite (Roberts et al., 2011). A hard coercivity component is present in sample B23-4, where about one third of the NRM remains after AF 65 mT. First-order reversal curve (FORC) diagrams for samples **(c)** B8 and **(d)** B23. The closed peak distribution indicates single domain (SD) magnetic particles (Roberts et al., 2014), which are stable remanence carriers.

and warm climate pollen taxa (Fig. 7). This suggests that these parameters will help to differentiate between cold and warm climate states. PCA axis 2 (18 % explained variance) separates samples with cool climate rainforest pollen taxa, high aquatic taxa (*Isoetes*, *Botryococcus*, and *Myriophyllum*) medium grain size, and higher carbonate values. This suggests that parameters on this axis will help to differentiate between wetter and drier climates.

6 Discussion

The core logging data and pilot multi-proxy analysis of the TAS1803 cores show a stratigraphy broadly in agreement with the first drillings at Darwin Crater (Howard and Haines, 2007) and provide exciting new insights into the nature and timing of lake sediment deposition. Two main lithotypes alternate throughout the 61 m thick lacustrine sediment succession; dark organic-matter-rich silts and olive-green siliciclastic silts. These lithotypes are interpreted as being deposited under interglacial and glacial climate conditions, based primarily on the NGR, spectrophotometry (L^* and b^*), LOI, and pollen data (Fig. 8). The olive-green silts, with higher NGR counts, relatively high L^* and b^* values, higher siliciclastic content, coarser grain size, and more abundant cold climate pollen taxa correspond to the sediments deposited during glacial periods. The brown-black silts with low NGR counts, relatively low L^* and b^* values, low sili-
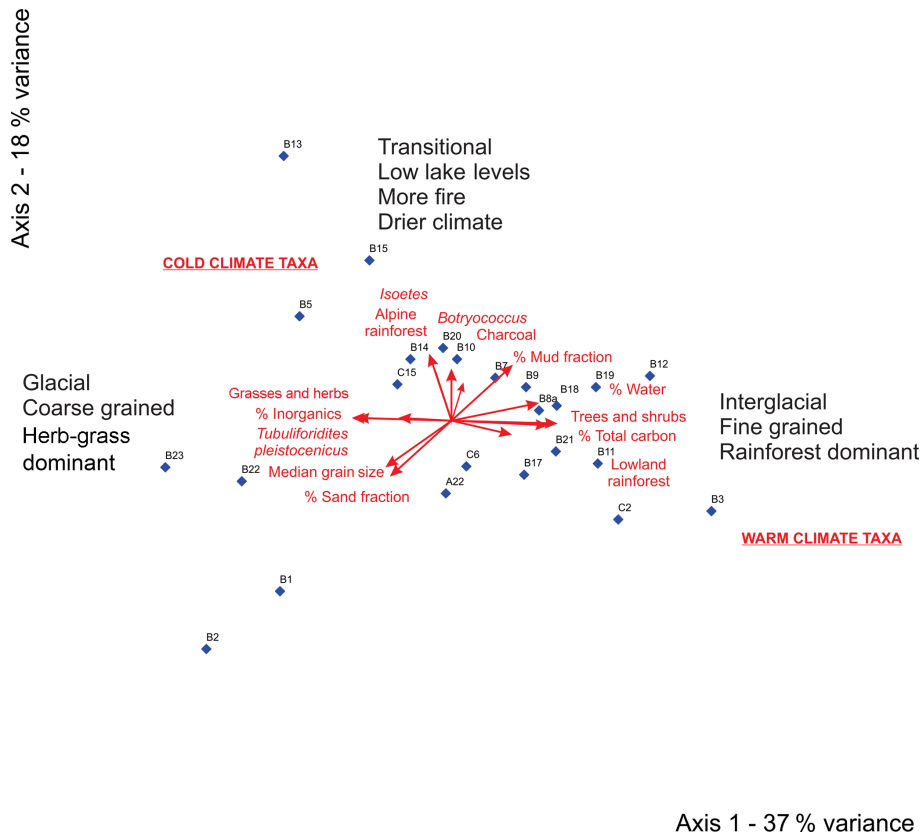
Figure 7. PCA bi-plot of core end data (pollen, LOI, and grain size). Correlations between data and axes $> 0.4 r^2$ are shown as red arrows (indicating the direction of correlation). A preliminary interpretation of the environmental significance of the axes is included.

ciclastic content, finer grains, and more abundant warm climate pollen taxa possibly correspond to sediments deposited during warm interglacial climate conditions (horizontal grey bars, Fig. 8). This is supported by the PCA of core end pollen and grain-size and LOI data, which indicate a principal gradient that separates samples that have coarse grains, low siliciclastic content, and pollen types indicative of a colder climate from samples that have fine grains, high organic content, and pollen types indicative of warmer climate conditions (Figs. 7 and 8j). These results are consistent with previous pollen studies, which indicate that glacial stages in western Tasmania are characterised by sparse open vegetation and poor organic soil development, which allows deposition of coarse siliciclastic sediment into lake basins (Beck et al., 2017; Colhoun, 2000; Colhoun et al., 1999). In contrast, interglacial periods in western Tasmania are characterised by maximum rainforest development, well-developed organic soils, and deposition of fine-grained and highly organic lake sediment (Beck et al., 2017; Colhoun, 2000; Colhoun et al., 1999).

The preliminary results of the Darwin Crater record suggest that the 61 m-thick lake deposit apparently covers a minimum of the seven full glacial cycles (interglacials tentatively highlighted in grey in Fig. 8). The length of each apparent

glacial cycle is variable, which may reflect different sedimentation rates, lake levels, and climate regimes through time. Similarly, the different grain-size distributions in the glacial olive silts (Fig. 5) may reflect changes in lake levels, sediment sources, availability, preservation, and/or climate regimes. High-resolution Itrax surface element scanning, multi-proxy analyses, and dating of the sediment archive (OSL, ^{36}Cl, U series, and magnetostratigraphy) are underway and will be used to precisely define, date, and determine how many climate cycles are present, especially in the lower part of the core where some proxies display high-frequency changes.

The preliminary results provide evidence for reducing conditions in the lake sediments. The visual observation of vivianite throughout the cores and the magnetic evidence for greigite (see GRM in Fig. 6a) imply reducing conditions. Moreover, framboidal pyrite was observed under the microscope in the basal core end samples at > 60 m depth (samples B21, A22, B22, and B23) as well as C6 (16.7 m). The magnetic susceptibility values are not null for these samples with pyrite, which suggests that iron oxides were not limiting the pyritisation process and/or that ferrimagnetic minerals formed sometime after pyrite formation. The k_{LF} variability, including intervals with near-zero values, does not seem
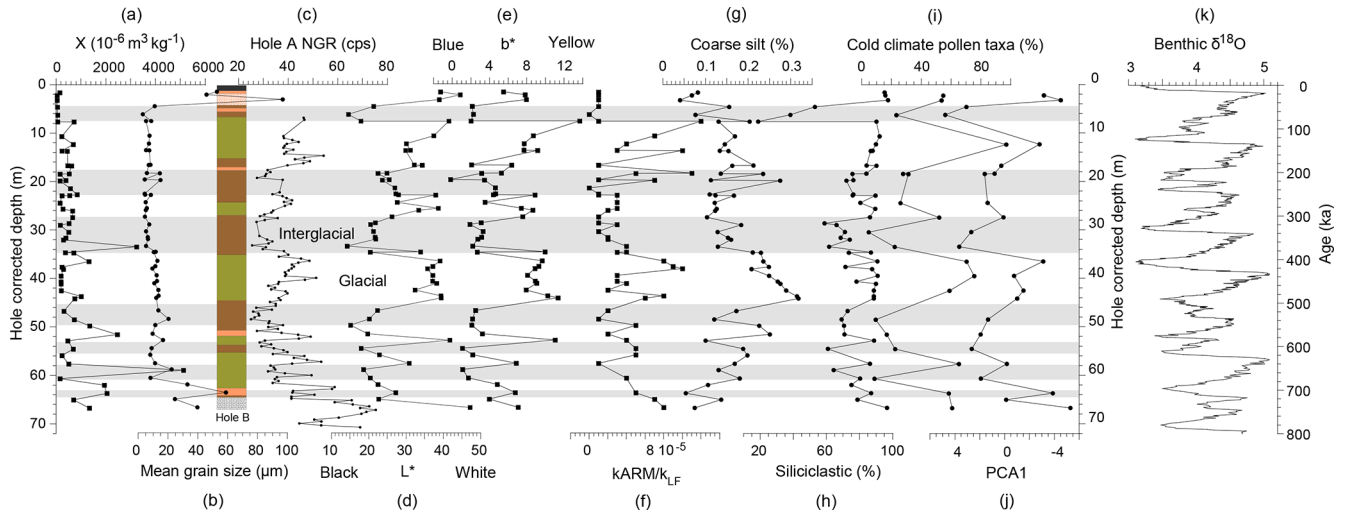
Figure 8. Selected parameters of the pilot multi-proxy analyses. **(a)** Mass-normalised magnetic susceptibility (χ), **(b)** mean grain size, **(c)** Natural gamma ray (NGR), **(d)** Color data L^* and **(e)** b^*, **(f)** Magnetic grain-size indicator kARM$/k_{LF}$, **(g)** coarse silt, **(h)** siliciclastic content, **(i)** cold climate pollen taxa, and **(j)** PCA axis 1 from left (warm) to right (cold). The starting and ending ages of the Darwin lacustrine sediment succession are unknown and will be identified by ongoing dating work. **(k)** A benthic δ^{18}O stack (Lisiecki and Raymo, 2005) is shown as a reference for Pleistocene glacial and interglacial climate cycles. A simplified lithology log for Hole B is included. The horizontal grey shaded bars tentatively indicate interglacial periods. Different symbols are used for different sample types: square symbols for measurements performed on the same cube samples, large circles for core end samples, and small circles for whole core MSCL samples.

correlated with the occurrence of pyrite, greigite, and vivianite. This suggests that factors other than the redox conditions may also control the k_{LF}, such as detrital input, biogenic iron oxides, their relative dilution in dia- and paramagnetic material, and/or chemical precipitation of magnetic minerals.

The lake in Darwin Crater formed sometime after 816 ± 7 ka (^{40}Ar$/^{39}$Ar dating of Darwin glass; Lo et al., 2002) and lake sedimentation terminated during a warm interglacial period which will be identified by ongoing dating work (Sect. 7). Pilot paleomagnetic analysis of the deepest core of Hole B (cube samples TAS1803-B23-MB-1, -2, -3, and -4) indicate normal magnetic polarity 1 m under the lake deposit (Fig. 6b). If this remanence was acquired at the time of deposition, this result constrains the entire lacustrine deposition to an age younger than 773 ka (Matuyama-Brunhes geomagnetic reversal; Ogg, 2012; Singer, 2014), which is consistent with the inferred interpretation of seven glacial cycles discussed above. Ongoing paleo- and environmental magnetic investigations aim to characterise the complex magnetic mineral assemblage, investigate reducing diagenesis, and build a full-vector paleomagnetic field record and paleoclimate proxies.

7 Future plans

The next stages of the project will focus on producing a chronologically constrained paleoclimate record. Core splitting of Holes A and C, Itrax XRF scanning, and subsampling for the planned multi-proxy analyses are underway, and col-

laborators have been engaged for testing and development of other sediment proxies, such as beryllium isotopes, diatoms, Cladocera, aDNA, and stable isotopes.

7.1 Planned analyses

7.1.1 Dating

Our immediate focus is on building a robust chronostratigraphy including OSL dating of quartz and feldspar grains in the sandy deposits, ^{36}Cl in the pre-lake deposits, uranium–thorium dating of vivianite, and radiocarbon dating of the uppermost sediments. There is potential for a full-vector paleomagnetic record combining remanent magnetisation and cosmogenic nuclide beryllium-10 (^{10}Be) for relative dating, using the global geomagnetic dipole field at the millennial scale (eg., Channell et al., 2009; Ziegler et al., 2011; Simon et al., 2016), and for independent comparison to paleoclimate records, including other continental records, marine sediments, and ice cores (via cosmogenic isotopes). The preliminary pollen data indicate potential targets for a tuning approach to changes in orbital geometry and associated insolation changes and global-scale climate records such as the LR04 benthic oxygen isotope stack (Fig. 8k; Lisiecki and Raymo, 2005).

7.1.2 Paleoclimate

For paleoclimate reconstructions, we are planning to employ a multi-proxy and high-resolution approach combining physical and biogenic indicators, including pollen, charcoal, magnetic properties, grain size, stable isotopes, and elemental composition. The long record of the Darwin Crater will be combined with a long record (2–3 glacial cycles; unpublished data) from neighbouring Lake Selina (location in Fig. 1) to help to establish a long and continuous continental record in Australia and one of the oldest in the Southern Hemisphere. The proxy dataset will then be used to test global climate model simulations to help understand climate dynamics and interactions (e.g. Menviel et al., 2014; Pedro et al., 2018).

7.2 Questions that will be addressed

The multi-proxy dataset will be collectively applied to address the main question motivating this project: what is the role of the SWWs in the Pleistocene climate cycles? In particular, we will investigate the following questions:

- How did the SWWs respond during the transition from glacial to interglacial climates (e.g. terminations), and what were the environmental impacts of these changes in Western Tasmania?

- Are inferred changes in SWW position or intensity related to changes in the concentration of atmospheric CO_2 over glacial cycles, and can these be related to changes in the capacity of the Southern Ocean CO_2 sink?

- Do the SWWs shift equatorward during glacial phases (Toggweiler et al., 2006; Toggweiler, 2009)?

- Do the SWWs display the proposed pattern of poleward contraction and the coupling with North Atlantic climate variability during terminations (Denton et al., 2010)?

- What is the environmental impact of the middle Pleistocene transition (if recorded) on the terrestrial environment in the southern mid-latitudes?

It is anticipated that the new lake sediment paleoclimate record from the mid-latitude Australian region will constitute an empirical test for conceptual models of SWW dynamics and provide essential boundary conditions for predictive climate models.

References

Allen, J., Cosgrove, R., and Garvey, J.: Optimality models and the food quest in Pleistocene Tasmania, J. Anthropol. Archaeol., 44, 206–215, 2016.

Barton, C.: Paleomagnetism, Age of the Darwin Crater, Bureau of Mineral Resources Yearbook, 36–37, 1987.

Beck, K. K., Fletcher, M.-S., Gadd, P. S., Heijnis, H., and Jacobsen, G. E.: An early onset of ENSO influence in the extra-tropics of the southwest Pacific inferred from a 14 600 year high resolution multi-proxy record from Paddy's Lake, northwest Tasmania, Quaternary Sci. Rev., 157, 164–175, 2017.

Blott, S. J. and Pye, K.: GRADISTAT: a grain size distribution and statistics package for the analysis of unconsolidated sediments, Earth Surf. Proc. Land., 26, 1237–1248, 2001.

Channell, J. E. T., Xuan, C., and Hodell, D. A.: Stacking paleointensity and oxygen isotope data for the last 1.5 Myr (PISO-1500), Earth Planet. Sci. Lett., 283, 14–23, 2009.

Colhoun, E. A.: Vegetation and climate during the last interglacial–glacial cycle in western Tasmania, Australia, Palaeogeogr. Palaeocl., 155, 195–209, 2000.

Colhoun, E. A. and van der Geer, G.: Pollen analysis of 0–20 m at Darwin Crater, western Tasmania, Australia, International Project of Paleolimnology and Late Cenozoic Climate, 11, 68–89, 1998.

Colhoun, E. A., Pola, J. S., Barton, C. E., and Heijnis, H.: Late Pleistocene vegetation and climate history of Lake Selina, western Tasmania, Quatern. Int., 57–58, 5–23, 1999.

Denton, G. H., Anderson, R. F., Toggweiler, J. R., Edwards, R. L., Schaefer, J. M., and Putnam, A. E.: The last glacial termination, Science, 328, 5986, https://doi.org/10.1126/science.1184119, 2010.

Egli, R.: VARIFORC: An optimized protocol for the calculation of non-regular first-order reversal curve (FORC) diagrams, Global Planet. Change, 110, 302–320, 2013.

Falster, G., Tyler, J., Grant, K., Tibby, J., Turney, C., Löhr, S., Jacobsen, G., and Kershaw, P. A.: Millenial-scale variability insoutheast Australian hydroclimate between 30 000 and 10 000 years ago, Quaternary Sci. Rev., 192, 106–122, 2018.

Faegri, K. and Iversen, J. (Eds.): Textbook of pollen analysis, Wiley, New York, 1989.

Fletcher, M.-S. and Thomas, I.: Modern pollen–vegetation relationships in western Tasmania, Australia, Rev. Palaeobot. Palyno., 146, 146–168, 2007.

Fudali, R. F. and Ford, R. J.: Darwin glass and Darwin Crater: A progress review, Meteoritics, 14, 283–296, 1979.

Garreaud, R. D.: Precipitation and circulation covariability in the extratropics, J. Climate, 20, 4789–4797, 2007.

Goetz, C. and Hillaire-Marcel, C.: U-series disequilibria in early diagenetic minerls from Lake Magali sediments, Kenya: Dating potential, Geochim. Cosmochim. Ac., 56, 1331–1341, 1992.

Gueguen, Y. and Palciauskas, V. (Eds.): Introduction to The Physics of Rocks, Princeton Universiy Press, UK, 1994.

Guyard, H., St-Onge, G., Pienitz, R., Francus, P., Zolitschka, B., Clarke, G. K. C., Hausmann, S., Salonen, V.-P., Lajeunesse, P., Ledoux, G., and Lamothe, M.: New insights into Late Pleistocene glacial and postglacial history of northernmost Ungava (Canada) from Pingualuit Crater Lake sediments, Quaternary Sci. Rev., 30, 3892–3907, 2011.

Harrison, R. J. and Feinberg, J. M.: FORCinel: An improved algorithm for calculating first-order reversal curve distributions using locally weighted regression smoothing, Geochem. Geophy. Geosy., 9, Q05016, https://doi.org/10.1029/2008GC001987, 2008.

Heiri, O., Lotter, A. F., and Lemcke, G.: Loss on ignition as a method for estimating organic and carbonate content in sediments: reproducibility and comparability of results, J. Paleolimnol., 25, 101–110, 2001.

Howard, K. T.: Physical trends in Darwin glass, Meteorit. Planet. Sci., 44, 115–129, 2009.

Howard, K. T. and Haines, P. W.: The geology of Darwin Crater, western Tasmania, Australia, Earth Planet. Sc. Lett., 260, 328–339, 2007.

Kalnay, E., Kanamitsu, M., Kistler, R., Collins, W., Deaven, D., Gandin, L., Iredell, M., Saha, S., White, G., Woollen, J., Zhu, Y., Chelliah, M., Ebisuzaki, W., Higgins, W., Janowiak, J., Mo, K. C., Ropelewski, C., Wang, J., Leetmaa, A., Reynolds, R., Jenne, R., and Joseph, D.: The NCEP/NCAR 40-year reanalysis project, B. Am. Meteorol. Soc., 77, 437–470, 1996.

Ledru, M.-P., Reimold, W. U., Ariztegui, D., Bard, E., Crósta, A. P., Riccomini, C., and Sawakuchi, A. O.: Why deep drilling in the Colônia Basin (Brazil)?, Sci. Dril., 20, 33–39, https://doi.org/10.5194/sd-20-33-2015, 2015.

Lisiecki, L. E. and Raymo, M. E.: A Pliocene-Pleistocene stack of 57 globally distributed benthic δ^{18}O records, Paleoceanography, 20, PA1003, https://doi.org/10.1029/2004PA001071, 2005.

Lo, C.-H., Howard, K. T., Chung, S.-L., and Meffre, S.: Laser fusion argon-40/argon39 ages of Darwin impact glass, Meteorit. Planet. Sci., 37, 1555–1562, 2002.

Macphail, M. K., Jordan, G. J., and Hill, R. S.: Key Periods in the Evolution of the Flora and Vegetation in Western Tasmania I. the Early-Middle Pleistocene, Aust. J. Bot., 4, 673–707, 1993.

Matchan, E. L., Philips, D., Traine, E., and Zhu, D.: 40Ar/39Ar ages of alkali feldspar xenocrysts constrain the timing of intraplate basaltic volcanism, Quat. Geochronol., 47, 14–28, 2017.

McLaren, S. and Wallace, M.: Plio-Pleistocene climate change and the onset of aridity in southeastern Australia, Global Planet. Change, 71, 55–72, 2010.

Melles, M., Brigham-Grette, J., Minyuk, P. S., Nowaczyk, N. R., Wennrich, V., DeConto, R. M., Anderson, P., Andreev, A. A., Coletti, A., Cook, T. L., Haltia-Hovi, E., Kukkonen, M., Lozhkin, A. V., Rosen, P., Tarasov, P., Vogel, H., and Wagner, B.: 2.8 Million years of Arctic climate change from Lake El"gygytgyn, NE Russia, Science, 337, 6092, https://doi.org/10.1126/science.1222135, 2012.

Menviel, L., Timmermann, A., Elison Timm, O., and Mouchet, A.: Deconstructing the Last Glacial termination: the role of millennial and orbital-scale forcings, Quaternary Sci. Rev., 30, 1155–1172, 2011.

Nuttin, L., Francus, P., Preda, M., Ghaleb, B., and Hillaire-Marcel, C.: Authigenic, detrital and diagenetic minerals in the Lagnua Potrok Aike sediment sequence, Quaternary Sci. Rev., 71, 109–118, 2013.

Ogg, J. G.: Geomagnetic Polarity Time Scale, Chapter 5, in: The Geologic Time Scale 2012, edited by: Gradstein, F. M., Ogg, J. G., Schmitz, M., and Ogg, G., Elsevier, 1176 pp., https://doi.org/10.1016/B978-0-444-59425-9.00005-6, 2012.

Pedro, J., Jochum, M., Cuisert, C., He, F., Barke, S., and Rasmussen, S. O.: Beyond the pipolar seesaw: Toward a process understanding of interhemispheric coupling, Quaternary Sci. Rev., 192, 27–46, 2018.

Peters, C. and Dekkers, M. J.: Selected room temperature magnetic parameters as a function of mineralogy, concentration and grain size, Phys. Chem. Earth, 28, 659–667, 2003.

Richardson, R. G.: Geophysical surveys of the Darwin Crater, Report UR1984_06, Mineral Resources of Tasmania, 1984.

Roberts, A. P, Heslop, D., Zhao, X., and Pike, C. R.: Understanding fine magnetic particle systems through use of first-order reversal curve diagrams, Rev. Geophys., 52, 557–602, https://doi.org/10.1002/2014RG000462, 2014.

Roberts, A. P., Chang, L., Rowan, C. J., Horng, C.-S., and Florindo, F.: Magnetic properties of sedimentary greigite (FeS4): an update, Rev. Geophys., 49, RG1002, https://doi.org/10.1029/2010RG000336, 2011.

Rothe, M., Kleeberg, A., and Hupfer, M.: The occurrence, identification and environmental relevance of vivianite in waterlogged soils and aquatic sediments, Earth-Sci. Rev., 158, 51–64, 2016.

Sagnotti, L.: Demagnetization Analysis in Excel (DAIE). An open source workbook in Excel for viewing and analyzing demagnetization data from paleomagnetic discrete samples and u-channels, Ann. Geophys.-Italy 56, 1–9, 2013.

Saunders, K. M., Roberts, S. J., Perren, B., Butz, C., Sime, L., Davies, S., Van Nieuwenhuyze, W., Grosjean, M., and Hodgson, D. A.: Holocene dynamics of the Southern Hemisphere westerly winds and possible links to CO_2 outgassing, Nat. Geosci., 11, 650–655, 2018.

Scholz, C. A., Karp, T., and Lyons, R. P.: Structure and morphology of the Bosumtwi impact structure from seismic reflection data, Meteorit. Planet. Sci., 42, 549–560, 2007.

Simon, Q., Thouveny, N., Bourlès, D. L., Valet, J. P., Bassinot, F., Ménabréaz, L., Guillou, V., Choy, S., and Beaufort, L.: Authigenic ^{10}Be / ^{9}Be ratio signatures of the cosmogenic nuclide production linked to geomagnetic dipole moment variation since the Brunhes/Matuyama boundary, J. Geophys. Res.-Sol. Ea., 121, 7716–7741, 2016.

Singer, B. S.: A Quaternary geomagnetic instability time scale, Quat. Geochronol., 21, 29–52, 2014.

Skinner, L. C., Fallon, S., Waelbroeck, C., Michel, E., and Barker, S.: Ventilation of the Deep Southern Ocean and Deglacial CO_2 Rise, Science, 328, 1147–1151, 2010.

Sniderman, K. J. M., Pillans, B., O'Sullivan, P. B., and Kershaw, A. P.: Climate and vegetation in southeastern Australia respond to Southern Hemisphere insolation forcing in the late Pliocene-early Pleistocene, Geology, 35, 41–44, 2007.

Stephens, T., Atkin, D., Augustinus, P., Shane, P., Lorrey, A., Street-Perrott, A., Nilsson, A., and Snowball, I.: A late glacial Antarctic climate teleconnection and variable Holocene seasonality at Lake Pupuke, Auckland, New Zealand, J. Paleolimnol., 48, 785–800, 2012.

Toggweiler, J. R.: Shifting Westerlies, Science, 323, 1434–1435, 2009.

Toggweiler, J. R., Russell, J. L., and Carson, S. R.: Mid-latitude westerlies, atmospheric CO_2, and climate change during the ice ages, Paleoceanography, 21, PA2005, https://doi.org/10.1029/2005PA001154, 2006.

Wilke, T., Wagner, B., Bocxlaer, B. V., Albrecht, C., Ariztegui, D., Delicado, D., Francke, A., Harzhauser, M., Hauffe, T., Holtvoeth, J., Just, J., Leng, M. J., Levkov, Z., Penkman, K., Sadori, L., Skinner, A., Stelbrink, B., Vogel, H., Wesselingh, F., and Wonik, T.: Scientific drilling projects in ancient lakes: Integrating geological and biological histories, Global Planet. Change, 143, 118–151, 2016.

Ziegler, L. B., Constable, C. G., Johnson, C. L., and Tauxe, L.: PADM2M: a penalized maximum likelihood model of the 0–2 Ma palaeomagnetic axial dipole moment, Geophys. J. Int., 184, 1069–1089, 2011.

Zolitschka, B., Anselmetti, F., Ariztegui, D., Corbella, H., Francus, P., Lücke, A., Maidana, N. I., Ohlendorf, C., Schäbitz, F., and Wastegård, S.: Environment and climate of the last 51000 years new insights from the Potrok Aike maar lake Sediment Archive Drilling prOject (PASADO), Quaternary Sci. Rev., 71, 1–12, 2013.